Description and performance of the Low Energy Transmission Grating Spectrometer on-board CHANDRA

Bert Brinkman, Theo Gunsing, Jelle Kaastra, Rob van der Meer, Rolf Mewe, Frits Paerels, Ton Raassen [1], Jan van Rooijen [a)], Heinrich Brauninger, Vadim Burwitz, Gisela Hartner, Gunther Kettenring, Peter Predehl [b)], Jeremy Drake, C. Olivia Johnson, Almus Kenter, Ralph Kraft, Stephen Murray, Peter Ratzlaff, Bradford Wargelin [c)]

[a)] Space Research Organization of the Netherlands (SRON), Sorbonnelaan 2, 3584 CA Utrecht, The Netherlands,
[b)] Max-Planck-Institut für extraterrestrische Physik, (MPE), Postfach 1603, D-85740 Garching, Germany
[c)] Harvard-Smithsonian Center for Astrophysics, 60 Garden Street, Cambridge, MA 02138, USA

ABSTRACT

The Chandra spacecraft has been launched successfully on July 23, 1999. The payload consists of a high resolution X-ray telescope (HRMA), two imaging detector systems in the focal plane and two transmission gratings. Each one of the two gratings can be put in the beam behind the telescope and the grating spectrometers are optimized for high and low energy, respectively. The Low Energy Transmission Grating Spectrometer (LETGS) consists of three parts: the high-resolution telescope, the transmission grating array and the detector, to read-out the spectral image.

A number of calibration measurements have been carried out since the launch, to verify and calibrate the spectrometer performance; mainly the resolution ($\Delta\lambda$ = 0.06 Å, FWHM) and wavelength scale accuracy. Calibration of the effective area of the spectrometer is an ongoing process. The long wavelength efficiency response (λ > 60 Å) has been established using the white dwarf star Sirius-B. The wavelength range shortwards of 60 Å is currently being verified using different astronomical sources with a "known" continuum spectrum.

Keywords: X-rays, spectrometer, CHANDRA

1. INTRODUCTION

The LETGS consists of three parts; the HRMA, the LETG and a detector system, to read-out the spectral image. In principle, the High Resolution Camera (HRC-S) as well as the Advanced CCD Imaging Camera (ACIS-S) can be selected. The ACIS-S detector has the advantage of intrinsic energy resolution, which makes it easy to separate the overlapping spectral orders on the detector. However, the limited physical size of the ACIS-S camera constrains the detectable wave range with the LETG to about 65 Å, whereas the HRC-S covers the range up to 170 Å. We therefore limit ourselves here to the LETG/HRC-S description, although a few LETG/ACIS-S calibration measurements have been carried out to cross calibrate the detectors.

Since the HRMA and HRC-S detector will be discussed in this section elsewhere, we will limit the description to the LETG. The LETG has been built in a collaborative effort between the Space Research Organization of the Netherlands (SRON) in Utrecht, The Netherlands [1,2] and the Max-Planck Institut für Extraterrestrische Physik (MPE) in Garching, Germany [3].

The principle of the "toroidal-Rowland geometry" [4] of a transmission grating spectrometer, utilizing a grazing incidence X-ray telescope, is shown in figure 1, and is briefly summarized below. X-rays, incident from the left, are reflected off the paraboloid and hyperboloid sections of the telescope. The resulting convergent beam falls onto the diffractor with center (vertex) 0. Its zero order F_0 is identical to the telescope focus. The distance between grating center and telescope focus is $0F_0 = x_0$. The circle through F_0, 0 with radius $x_0/2$ is the Rowland circle. The torus generated by rotating the Rowland circle

[1] Also at Astronomical Institute "Anton Pannekoek", Kruislaan 403, 1098 SJ Amsterdam, The Netherlands.

In *X-Ray Optics, Instruments, and Missions III*, Joachim E. Trümper, Bernd Aschenbach, Editors,
Proceedings of SPIE Vol. 4012 (2000) • 0277-786X/00/$15.00

around the z-axis is called the Rowland torus. Each grating element is mounted with its center on the Rowland torus and with its plane perpendicular to the incoming X-ray beam from the telescope. The grating wires lie in planes perpendicular to z. For a specific wavelength, the diffractor also produces first (and higher) orders, plus and minus, at positions F_{+1} and F_{-1} on the Rowland torus. For rays falling onto the center of each grating element, these images are sharp astigmatic lines perpendicular to the dispersion axis z. This ideal Line Spread Function is only correct for the grating center and thus for infinitesimally small grating elements. In reality only a finite number of grating elements can be accommodated, and a small widening of the astigmatic line will result.

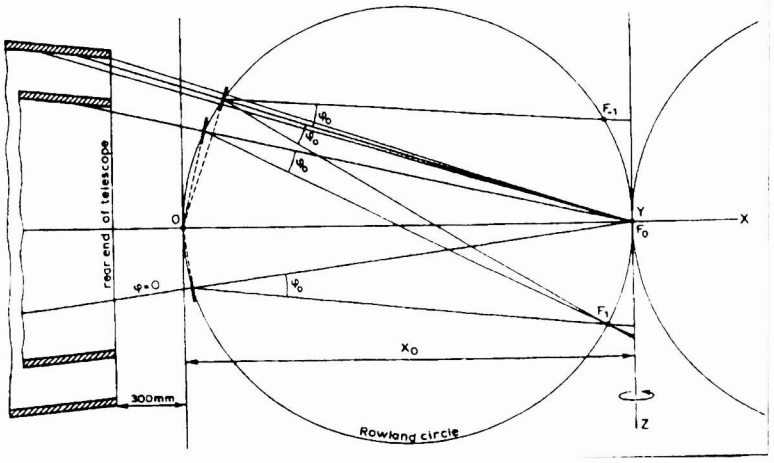

Figure 1: Toroidal grating. The grating elements are mounted on the toroid, generated by rotating the Rowland circle about the z-axis.

The beam area behind each one of the four co-aligned concentric mirrors is covered by a large number of circular grating facets with 1.5 cm diameter each. Three facets have been integrated into one element. The facets within each element are co-aligned. One hundred eighty elements are needed to cover the total telescope beam, whereby the alignment of the facets on each element differ from element to element, in order to achieve the required co-alignment of the gratings.

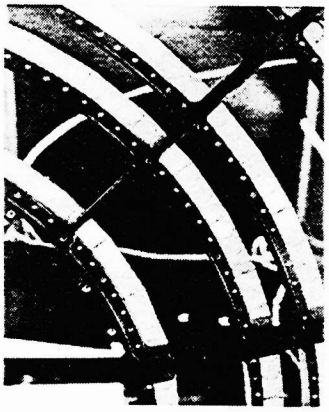

Figure 2: Part of LETG with modules containing three grating facets each.

The prime detector, to read out the LETG image, is the HRC-S detector. The detector consists of three ten cm long segments whereby the outer two are tilted slightly with respect to the center one in order to approximate the Rowland circle.

The nominal zero order focus point on the central strip detector is moved 4 mm away from the center, along the dispersion direction. This asymmetry is created to avoid that the two small dead areas between the center detector strip and the outside strips, block the same spectral band on the spectral orders. See figure 3, cross section of HRC-S detector.

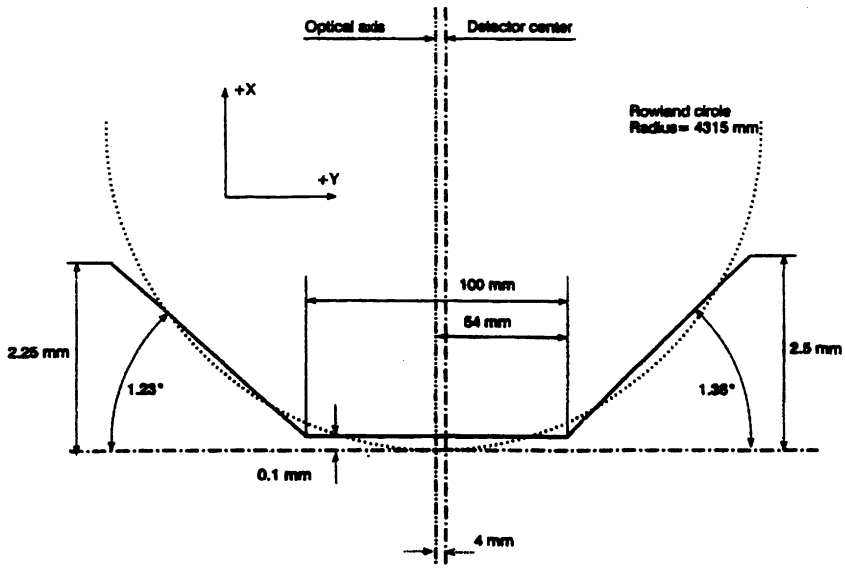

Figure 3: Cross-section of the HRC-S strip detector, not to scale.

The angular dispersion relation for a grating of this type is:

$$\sin\phi_i - \sin\phi_o = m\lambda / d, \tag{1}$$

with ϕ_i the incident angle, ϕ_0 the dispersion angle in the dispersed plane with respect to the optical axis, m the spectral order, λ the wavelength and d the grating period. The total wavelength range that can be covered simultaneously, assuming the zero order falls in the center of the detector, is determined by the detector size.

The linear dispersion is given by:

$$z = x_o \frac{m\lambda}{d}. \tag{2}$$

The grating spectrometer resolving power for the first order becomes:

$$\frac{\lambda}{\Delta\lambda} = \frac{x_0}{d} \cdot \frac{\lambda}{\Delta z}, \tag{3}$$

Here Δz is the width of the LSF of the LETGS.

The expression for the resolution can be written as follows, assuming that the different contributions to Δz can be added quadratically

$$\frac{\lambda}{\Delta\lambda} = x_0 \frac{\lambda}{d} \left\{ (f\Delta\theta)^2_{HRMA} + \Delta z^2_{DET} + \Delta z^2_{GR} \right\}^{\frac{1}{2}}, \tag{4}$$

where f is the focal length of the telescope, $\Delta\theta$ is the telescope resolution, including attitude reconstruction errors. Δz_{DET} is the detector position resolution and Δz_{GR} the grating resolution in the focal plane. Obviously, optimum focussing is assumed.

2. THE FIRST LIGHT X-RAY SPECTRUM

The preliminary in-flight resolution and wavelength scale calibration has been obtained from the first light measurements of the nearby star Capella. Capella is a binary system at a distance of 12.9 pc comprised of G8 and G1 giants with an orbital period of 104 days. It is the brightest quiescent coronal X-ray source in the sky after the sun, and is therefore an obvious line source candidate for first light observations and for instrument calibration. X rays from Capella were discovered [5,6] in 1975 and subsequent satellite observations provided evidence for a multi-temperature component plasma.

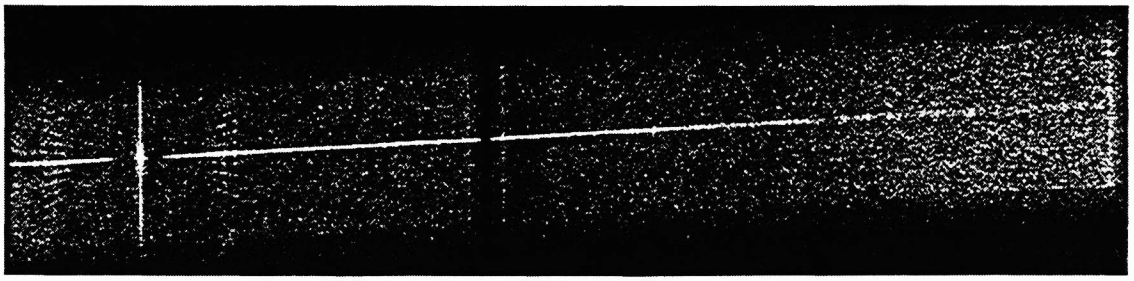

Figure 4: Spectral image of Capella.

Figure 4 shows the detector image after it has been corrected for spacecraft attitude drift and after dedithering. (During a pointing, the spacecraft is moved over the sky in a controlled fashion to avoid that all photons from a celestial point source are imaged into one detector pixel; this process of controlled movement is called dithering).

The bright horizontal line is the dispersed spectrum. The bright spot on the left side is the central zero order (not the full three detector elements have been shown).
The bright vertical line through the zero order is caused by the fine support structure, with wires perpendicular to the main grating. The fine support structure also acts as a grating and has a period of about 25 μm. It is interesting to note that one can see this support structure also above and below the main spectrum. In the cross dispersion direction, the spectral width is minimal at 0^{th} order and increases at longer wavelengths due to the intrinsic astigmatism of the Rowland circle spectrograph.
The main grating dispersion is 1.15 Å/mm in first spectral order as determined by the instrument geometry and grating line density.

Converting the spectral image into a spectrum is done by applying a spatial extraction box around the spectral image and constructing a histogram of counts versus position along the dispersion direction. The extraction box in the cross dispersion direction needs to be as small as possible to reduce the background, without taking away a substantial part of the photon distribution. This is particularly important because the anti-coincidence circuit in the HRC-S, to reject background, doesn't work. In addition some further background suppression is possible by rejecting the highest and lowest energy events of the event pulse height distribution. That way about one third of the background can be eliminated in principle. A difficulty is that the pulse height distributions vary over the face of the detector box and need to be calibrated. The background level is estimated from areas on the detector away from the spectral image.

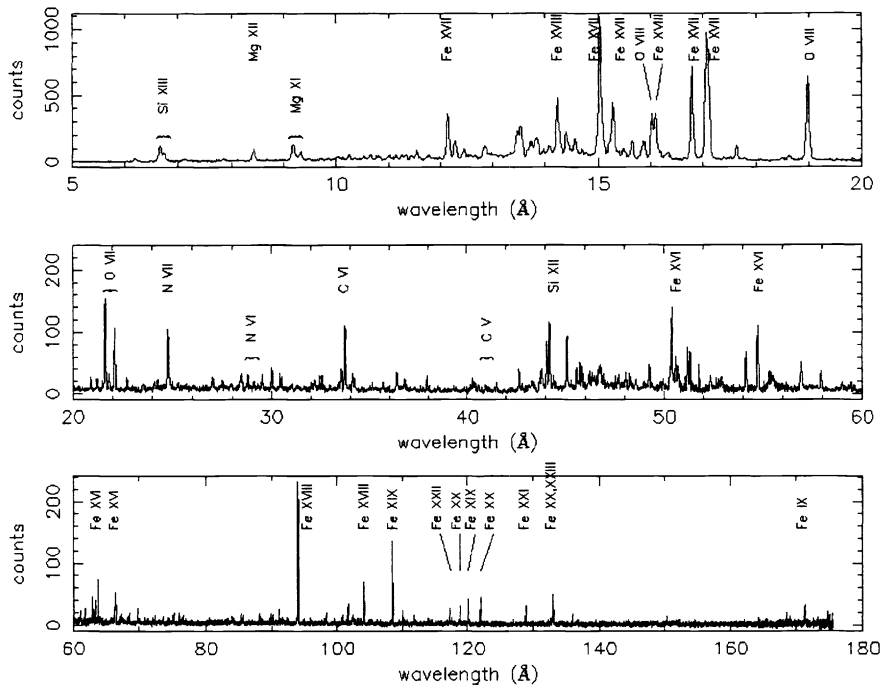

Figure 5: The complete LETGS spectrum of Capella, split into three parts for clarity. Note the difference in X and Y scale for the three parts.

The thus extracted spectrum is shown in figure 5 and was accumulated in about 85 ks [5]. From the intrinsic narrow lines the resolution can be measured directly and was found to be 0.06 Å, FWHM. This is about as predicted from design considerations and from the payload ground system test at the long beam X-ray test facility in Huntsville.

3. WAVELENGTH SCALE CALIBRATION

For the complete HRC-S, the Capella spectrum has been analyzed in terms of the quantity $m\lambda_{observed} - m\lambda_{predicted}$ as a function of wavelength. The analysis involves 171 lines in the data set, and relates to both positive and negative orders. We tried to analyze the above quantity in terms of decenter (of the 0^{th} order along the dispersion axis), plate scale (conversion pixel or angle to wavelength) for the central detector element, off-sets (jumps) at the detector boundaries, and plate scales (or inclination angles) for the outer detector elements.

The procedure is as follows. First the centroid of "unblended lines" was determined by a quasi-automatic fitting procedure. Then, the line was identified, using existing literature. In addition to statistical errors on the line centroids, we also included an uncertainty in the theoretical wavelength, as follows: 0.001 Å for the H and He-like lines, 0.003 Å for other lines with λ < 20 Å, all other lines 0.01 Å, and for higher orders *m* times the first order error. We fitted straight lines to the date for each of the three detector elements:

$$m * \left(\lambda_{obs} - \lambda_{pred}\right) = A + B * \lambda_{pred}, \tag{5}$$

where *m* the spectral order, λ_{obs} the measured wavelength, λ_{pred} the theoretical wavelength including errors and with A and B as free parameters. This process was done for six different data sets of Capella. The constant B for the outer detector segments was (1.32 ± 0.10) x 10^{-3} Å/Å and for the central segment (0.56 ± 0.03) x 10^{-3} Å/Å.

Furthermore:

$$A\ S(1) - A\ S(2) = (-22 \pm 3)\ 10^{-3}\ \text{Å}$$
$$A\ S(3) - A\ S(2) = (-41 \pm 3)\ 10^{-3}\ \text{Å}$$

These shifts represent corrections in the gap size between outer and central plate.

After applying these corrections, the wavelength difference as a function of "true wavelength" still shows some systematic effects.

It is clear that the remaining errors are not random and are probably related to non-uniformities of the detector. Assuming this to be the case, we may be able to calibrate these "large scale non-uniformities". If these appear to be stable with time, the wavelength uncertainty could probably be reduced to about 10 mÅ.

4. LETGS EFFECTIVE AREA

4.1. Introduction

In order to measure absolute fluxes of celestial X-ray sources it is necessary to know the effective area of the LETGS, to be able to convert detector counts into source photons. Establishing the effective area is a long process which starts with calibrating the different subsystems that make up the LETGS, being the HRMA, LETG and HRC-S. For all three components, models have been generated which were tested to some extent at subsystem level. Then a payload system test (XRCF-test, dec. 1996-april 1997) was carried out. We are now in the phase of verifying/calibrating the models with astrophysical sources. This is not straightforward because there are no relatively strong point sources with a constant intensity and with a well established spectrum over the full range. It is beyond the scope of this paper to summarize all relevant tests of HRMA, LETG and HRC-S. For the performance of HRMA and HRC-S we refer to the Chandra Calibration Website and the papers in this conference session. The LETG model based on pre-flight tests, grating sample tests as well as XRCF-tests, is discussed hereafter.

The transmission grating efficiency can be modelled in terms of the geometrical characteristics of the grating as, for instance, grating wire thickness, width, and the refractive index of the grating material. In the most simple case of a rectangular cross section of the grating wire, the efficiency of a given diffraction order (i.e., the fraction of incoming radiation diffracted into that order) is represented by

$$\frac{I^m}{I_0}(\lambda) = \left[\frac{\sin\left(m\pi\frac{a}{d}\right)}{m\pi}\right]^2 \left[1 + e^{-\frac{4\pi}{\lambda}\beta z} - 2e^{-\frac{2\pi}{\lambda}\beta z}\cos\left(\frac{2\pi}{\lambda}\delta z\right)\right], \tag{6}$$

with: m = diffraction order (for m ≠ 0), d = grating period, a = gap between grating wires, z = wire thickness, λ = wavelength, β = imaginary part of the refractive index, and δ = real part of the refractive index [8].

The second term plays only a role if the grating wires are partially transparent. In case of full transparency, they obviously do no longer act as grating; in the case of fully opaque grating bars, the second term is 1 and the efficiency is only determined by the width of the wires. The second term can be much larger than 1, at least within limited wavelength bands, if the thickness is adjusted appropriately. In an optimum case (a/d = 0.5) the first order efficiency reaches a maximum and all even orders are suppressed.

For a rectangular wire cross-section, the efficiency-ratios of all orders (m ≥ 1) are constant, independent of the wavelength. We observe, however, that particularly in wavelength regimes where the grating is partially transparent, these ratios vary. This indicates that the rectangular representation of the grating wires is too simple; the next logical step would be the

representation by a trapezoid[9]. Now depending on the transparency of the grating, the 'effective' width of the wire varies, and the efficiency ratios vary as well. This can lead to a complicated behaviour, particularly for those orders which are almost suppressed.

At the beginning of the LETG program we realised that testing of all grating samples (~ 1500 for flight, spare and all test purposes) in the laboratory X-ray test facility would be a horrendous task. Therefore we have developed a novel method based on the transmissivity of a grating for polarised light in the so-called resonance domain, i.e. the wavelength range around the grating period [10]. This is, in our case, the Near-Infrared region at 1μm. This method was validated both by electron microscope studies [11] and X-ray measurements on so-called 'Performance Verification Samples' (PVS), ten randomly selected facets.

During the payload system tests in NASA-MSFC's long beam X-ray test facility (XRCF) in Huntsville/Al the LETG could be tested for the first time in X-rays in the convergent beam behind the Chandra High Resolution Mirror Assembly (HRMA). The correct geometry and co-alignment of the 540 grating facets had been verified before with a laser set-up in the MPE- and SRON-laboratories.

Although the results of the complex tests at XRCF were not always easy to interpret, it became nevertheless apparent that there were significant deviations between model and data particularly at wavelength < 10Å. Here, the grating is partially transparent, and the efficiency in the diffraction orders depends strongly on the wavelength. Deviations of up to 30% occurred, much beyond our accuracy goals. We therefore re-measured very accurately the PVS gratings in X-rays in an effort to recalibrate the NIR-data. These measurements were performed at the synchrotron light source DESY in Hamburg for the longer wavelength range and MPE's long beam test facility PANTER for the shorter wavelength range.

Unfortunately, after this exercise, we still could not fit all data of an individual grating consistently with the trapezoidal model. In a second approach, we tried to fit the data independently for the different diffraction orders. It turned out that the width of the grating wires was fairly well represented by the NIR-method although the results scattered slightly around the nominal value. The thickness was generally underestimated. The most interesting result, however, was that the thickness seems to "depend on diffraction order". This suggests an underlying physical effect not considered so far.

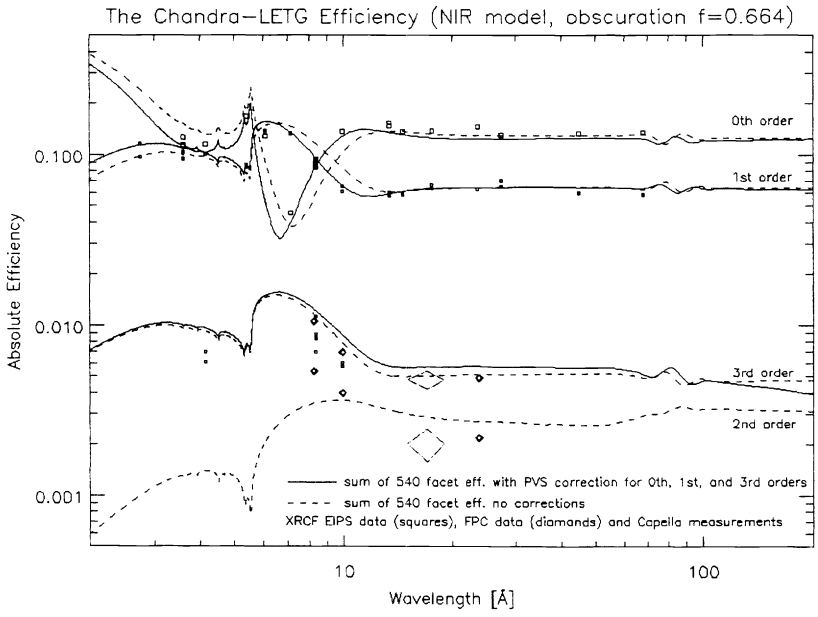

Figure 6: The absolute efficiency (including all actual vignetting for on-axis pointing) of LETG as a function of wavelength. For explanation see text.

Based on this exercise, we have 'fudged' the NIR-data by adding constants to the wire width, thickness and slope of the assumed mean trapezoidal cross sections of each grating. Then we generated the corrected model based on the above modifications. Figure 6 shows the absolute zero, first, second and third order model efficiency. The solid line represents the correction discussed above and the dotted line is the uncorrected version. For the second order (lowest curve) only the uncorrected version is shown. The squares are measured points from XRCF-measurements. The diamonds represent relative measurements (ratio of third to first and of second to first order) from XRCF. In order to place the relative measurement points in the absolute efficiency plots, the points were multiplied with the first order efficiency at that wavelength. The wide diamonds represent actual flight data from Capella, treated like the XRCF ratio data. The Capella data represents strong lines closely together (15.02, 17.05, 17.10 and 18.96 Å) and are shown here as one data point.

By using the relative XRCF data and further flight data, we expect to be able to establish the higher order efficiencies to the required level.

4.2. LETGS Low Energy Efficiency calibration using Sirius-B

The long wavelength response, beyond the Carbon-edge at about 40 Å, is not well known mainly due to the uncertainty in HRC-S detector efficiency.

The effective area of the complete spectrometer can be established by using a strong soft point source. Sirius-B is the best candidate for this. Martin Barstow and recently Heise and Barstow have looked carefully into the existing white dwarf model and estimated the flux uncertainty to be smaller than 10%. The hereafter preliminary derived effective area is therefore directly coupled to our knowledge of the Sirius-B absolute flux. Fig 7a shows the input spectrum as used for this calibration. Since the source has very little flux shortwards of 60 Å, there is no concern about higher order contamination at longer wavelengths. Important for absolute effective area determination is the exact size of the detector extraction box in the cross dispersion direction, to generate the spectrum. With too narrow a box, one cuts into the X-ray distribution and with too wide an extraction box, we include much background and therefore the errors get larger. In order to determine the optimum size of the extraction box, we used data from HZ43, which is a much stronger source (with less wellknown absolute spectra). HZ43 can be used to verify the relation between included X-ray flux vs. extraction box size. It appears that a box, which includes 90% of the X-ray flux, generates the best signal to noise.

Figure 7[b] shows the measured count rates as a function of wavelength. The data represents 12 ks of observation. The best fit solid line is the model times "effective area" (90%). The derived effective area (first orders) are then shown in figure 7[c].

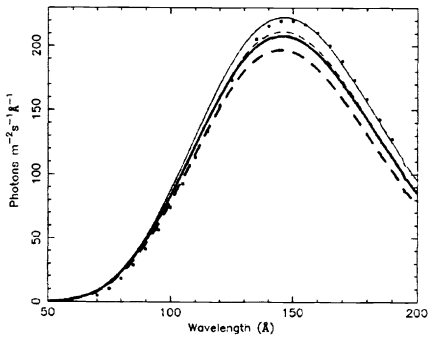

Figure 7a: Model spectra for Sirius-B. Dots: model as published by Holberg et al., 1998 [12]. Thick solid line: new model calculation determined by Heise and Barstow (private communication) based upon the parameters given by Holberg et al. Thin solid line: same model, but with the effective temperature 100 K larger. Dashed lines: as solid lines, but with increased surface gravity and decreased helium abundance.

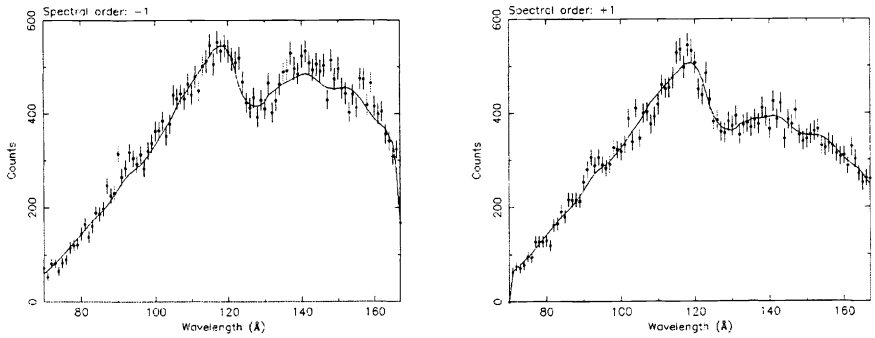

Figure 7b: Observed count spectrum of Sirius-B, binned into 1 Å bins, for left and right outer detector segment. Dots with error bars: observed spectrum. Solid line: model spectrum of fig a, multiplied by the corrected effective area of fig 7c.

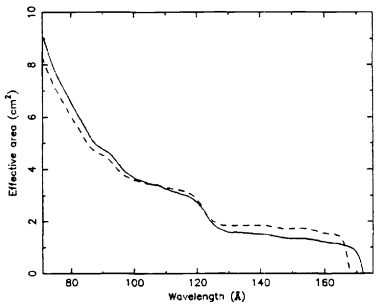

Figure 7c: Effective area for the outer plates of the LETGS as derived from the Sirius-B data. Dashed line: spectral order –1, solid line: spectral order +1.

4.3. LETGS medium energy efficiency calibration

The most straightforward way to verify the LETGS effective area is to use a continuum source with a well-defined spectrum and compare the predicted and actual results. An additional difficulty is that the HRC-S cannot separate the different spectral orders. The predicted count rate therefore consists of the contributions of the first and higher orders together. We are in the process now of doing this procedure by using a few different celestial sources and look for systematic deviations, which will then be attributed to the LETGS-response. One obviously needs a few sources with different spectra to disentangle the detector from grating effects. To help this process we also have measurements of LETG with ACIS-S. Furthermore looking at the same source with LETGS and HETGS well shed some light on possible remaining systematic effects. Of course it is foreseen to simultaneously measure a few targets with instruments on other spacecrafts such as SAX and XMM, to cross calibrate the spectrometers.

5. CONCLUSION

The LETGS performs very well. The resolving power (resolution) is very good and as expected from design considerations and from XRCF-tests. The measured low energy effective area is lower than predicted in the AXAF proposers guide by a factor of 1.6. However this new value was expected from the latest available HRC-S data prior to flight. The HRC-S detector background is very much higher than expected, due to an error in the veto system. This requires therefore extra careful evaluation of optimum size extraction boxes, and filtering. The detailed efficiency calibration is ongoing and converging.

ACKNOWLEDGEMENT

We like to express our gratitude to many people who have made the LETGS a success. This applies particularly to the hardware teams who built the different parts of the LETGS as well as the industrial team who built the spacecraft and the CXC who operates Chandra.

REFERENCES

[1] Brinkman, A.C., Rooijen, J.J. van, Bleeker, J.A.M., Dijkstra, J.M., Heise, J., Korte, P.A.J. de, Mewe, R., Paerels, F., *"Low Energy X-ray Transmission Grating Spectrometer for AXAF"*, in: X-ray Instrumentation in Astronomy, Proc. SPIE, Vol. 597, 232-241, 1985.

[2] Brinkman, A.C., Gunsing, C.J.Th., Kaastra, J.S., Bräuninger, H.W., Hartner, G.D., Predehl, P., Drake, J.J., Juda, J.Z., Dewey, D., Flanagan, K.A., Marshall, H.L., *"Preliminary Test results on spectral resolution of the Low Energy Transmission Grating Spectrometer on board of AXAF"*, in: Grazing Incidence and Multilayer X-ray Optical Systems, Proc. SPIE, Vol. 3113, 172-180, 1997.

[3] Predehl, P., Bräuninger, H.W., Brinkman, A.C., Dewey, D., Drake, J.J., Flanagan, K.A., Gunsing, T., Hartner, G.D., Juda, J.Z., Juda, M., Marshall, H.L., Swartz, D.A., *"X-ray calibration of the AXAF Low Energy Transmission Grating Spectrometer: effective area"* (invited paper) in: Grazing Incidence and Multilayer X-ray Optical Systems, Proc. SPIE, Vol. 3113, 181-192, 1997.

[4] Beuermann, K.P., Bräuninger, H. and Trümper, J., Applied Optics, Vol. 17, no. 15, 2304 (1978).

[5] Catura, R.C., Acton, L.W., and Johnson, H.M., 1975, ApJ, 196, L47.

[6] Mewe, R., Heise, J., Gronenschild, E.H.B.M., Brinkman, A.C., Schrijver, J., Boggende, A.J.F., 1975, ApJ, 202, L67.

[7] Brinkman, A.C., Gunsing, C.J.Th., Kaastra, J.S., Meer, R.L.J. van der, Mewe, R., Paerels, F., Raassen, A.J.J., Rooijen, J.J. van, *"First light measurements of Capella with the Low Energy Transmission Grating Spectrometer aboard the Chandra X-ray Observatory"*, 2000, Ap.J. Letters, in press.

[8] Schnopper, H.W., Van Speybroek, L.P., Devaille, J.P., Epstein,A., Källne,E., Bachrach, R.Z., Dijkstra, J., and Lantwaard, L. 1977, Appl. Opt. **16**, 1088.

[9] Bräuninger, H., Predehl, P. and Beuermann, K.P. 1979, Appl. Opt. **18**, 368

[10] Lochbihler, H., and Predehl, P., 1992, Appl. Opt. **31**, 964

[11] Lochbihler, H., Predehl, P., and Tesche, B., 1994, Optik **98**, 21

[12] Holberg, J. B.; Barstow, M. A.; Bruhweiler, F. C.; Cruise, A. M.; Penny, A. J., Astrophys. J. 497, 935 (1998)